

Roles of cooperative effects and disorder in photon localization: The case of a vector radiation field

L. Bellando^{1*}, A. Gero^{2,3}, E. Akkermans², and R. Kaiser¹

¹*Université de Nice Sophia Antipolis, CNRS, Institut Non-Linéaire de Nice, UMR 7335, F-06560 Valbonne, France*

²*Department of Physics, Technion - Israel Institute of Technology, 32000 Haifa, Israel*

³*Department of Education in Technology and Science,
Technion - Israel Institute of Technology, 32000 Haifa, Israel*

(Dated: December 16, 2024)

We numerically study photon escape rates from three-dimensional atomic gases and investigate the roles of cooperative effects and disorder in photon localization, while taking into account the vectorial nature of light. A scaling behavior is observed for the escape rates, and photons undergo a crossover from delocalization toward localization as the optical thickness of the cloud is increased. This result indicates that photon localization is dominated by cooperative effects rather than disorder. We compare our results with those obtained in the case of a scalar radiation field and find no significant differences. We conclude that the scalar model constitutes an excellent approximation when considering photon escape rates from atomic gases.

PACS numbers: 42.25.Dd, 42.50.Nn, 72.15.Rn

I. INTRODUCTION

Photon localization in cold atomic gases, namely an overall decrease of photon escape rates from the cloud, is a subject of interest in atomic and optical physics [1–4]. To investigate this phenomenon, two different approaches have been proposed. The first one studies the complex spectrum of the effective Hamiltonian describing the atomic system. Within this framework, the real part of an eigenvalue corresponds to the energy of the eigenstate, while its imaginary part is related to the decay rate [2, 5, 6]. In the second approach, photon escape rates are determined by the time evolution of the ground-state population obtained from the reduced atomic density matrix of the gas. This time evolution is governed by the spectrum of the imaginary part of the effective Hamiltonian [7–9].

Here, we follow the latter approach in order to compare the roles of disorder [10] and cooperative effects, e.g., superradiance and subradiance [11], in photon localization. It has been shown that in two- and three-dimensional media, photon localization occurs as a crossover between two limits: the single-atom limit where photons are spatially delocalized and spontaneous emission of independent atoms occurs, and the opposite limit where the photons are trapped in the gas for a very long time [9, 12]. As these two limits are connected by a crossover rather than a disorder-driven phase transition as expected from Anderson localization [13], one can argue that photon localization is dominated by cooperative effects rather than disorder. In one-dimensional atomic gases, the single-atom limit is never reached and photons are always localized in the cloud - a result clearly attributed to co-

operative effects [14]. It should be emphasized, however, that these studies have been restricted to the interaction of a scalar radiation field with the atoms.

In this paper we consider the more realistic case of a vector radiation field interacting with a three-dimensional atomic gas. We show that the vector and scalar models qualitatively lead to the same results. Moreover, in both cases a scaling behavior is observed for the escape rates and photons undergo a crossover from delocalization toward localization as the optical thickness of the cloud is increased.

The paper is organized as follows. In Section II, we present the model of a gas of identical atoms interacting with the radiation field. In Section III, the atomic effective Hamiltonian is introduced, and in Section IV the photon collective emission rates from the atomic cloud are derived. In Section V we describe our numerical methods, and in Sections VI-VII present our findings. We finally discuss our results in Section VIII and draw some conclusions in Section IX.

II. MODEL

Atoms are taken as identical two-level systems, a ground state $|g\rangle = |J_g = 0, m_g = 0\rangle$ and an excited state $|e\rangle = |J_e = 1, m_e = 0, \pm 1\rangle$. J is the quantum number of the total angular momentum and m is its projection on a quantization axis, taken as the \hat{z} axis. The states associated to m_e are spanned by the Cartesian basis $\{|\alpha\rangle\} = \{|x\rangle, |y\rangle, |z\rangle\}$, where $|x\rangle = \frac{1}{\sqrt{2}}(|-1\rangle - |1\rangle)$, $|y\rangle = \frac{i}{\sqrt{2}}(|-1\rangle + |1\rangle)$ and $|z\rangle = |0\rangle$. Therefore, further on we denote the excited state by $|e_\alpha\rangle$. The energy separation between the ground and excited states, including radiative shift, is $\hbar\omega_0$ and the natural width of the excited state is $\hbar\Gamma_0$.

In order to describe the dynamics of $N \gg 1$ atoms,

*Current affiliation : Université de Bordeaux, CNRS, LOMA, UMR 5798, F-33405 Talence, France.

distributed at random positions \mathbf{r}_i in an external radiation field, we use the Hamiltonian $H = H_0 + V$. H_0 is the free Hamiltonian, written as a sum of the atomic and radiation terms,

$$H_0 = \hbar\omega_0 \sum_{i=1}^N \sum_{\alpha} |e_{\alpha}^i\rangle \langle e_{\alpha}^i| + \sum_{\mathbf{k}\hat{\varepsilon}} \hbar\omega_k a_{\mathbf{k}\hat{\varepsilon}}^{\dagger} a_{\mathbf{k}\hat{\varepsilon}}. \quad (1)$$

Here, $a_{\mathbf{k}\hat{\varepsilon}}^{\dagger}$ ($a_{\mathbf{k}\hat{\varepsilon}}$) is the creation (annihilation) operator of a photon of wave vector \mathbf{k} ($\omega_k = c|\mathbf{k}|$) and polarization $\hat{\varepsilon}$ ($\mathbf{k} \cdot \hat{\varepsilon} = 0$).

The light-matter interaction V expressed in the electric dipole approximation is

$$V = - \sum_{i=1}^N \mathbf{d}_i \cdot \mathbf{E}(\mathbf{r}_i), \quad (2)$$

where $\mathbf{d}_i = e\mathbf{r}_i$ is the electric dipole moment operator of the i -th atom.

The atoms are coupled to each other via the electric field operator:

$$\mathbf{E}(\mathbf{r}) = i \sum_{\mathbf{k}\hat{\varepsilon}} \sqrt{\frac{\hbar\omega_k}{2\epsilon_0\mathcal{V}}} \left(a_{\mathbf{k}\hat{\varepsilon}} \hat{\varepsilon} e^{i\mathbf{k}\cdot\mathbf{r}} - a_{\mathbf{k}\hat{\varepsilon}}^{\dagger} \hat{\varepsilon}^* e^{-i\mathbf{k}\cdot\mathbf{r}} \right). \quad (3)$$

It is assumed that the typical speed of the atoms is small compared to Γ_0/k_0 but large compared to $\hbar k_0/\mu$, where μ is the mass of the atom and $k_0 = \omega_0/c$ is the wavenumber of the light used to probe the system. Under this assumption, the Doppler shift and recoil effects are negligible. Furthermore, we neglect retardation effects, so that interaction between atoms is instantaneous.

III. EFFECTIVE HAMILTONIAN

Performing the trace over the radiation degrees of freedom of H , while being restricted to the case of a single excitation, produces the non-Hermitian effective Hamiltonian [9, 15, 16]:

$$H_{eff} = \left(\hbar\omega_0 - i\frac{\hbar\Gamma_0}{2} \right) \sum_{i=1}^N \sum_{\alpha} |e_{\alpha}^i\rangle \langle e_{\alpha}^i| - \frac{\hbar\Gamma_0}{2} \sum_{i \neq j} \sum_{\alpha\beta} g_{\alpha\beta}(\mathbf{r}_{ij}) S_{i,\alpha}^{(+)} S_{j,\beta}^{(-)}, \quad (4)$$

where $S_{i,\alpha}^{(+)} = |e_{\alpha}^i\rangle \langle g^i|$ is the raising operator of the i -th atom along the α direction and $S_{i,\alpha}^{(-)} = [S_{i,\alpha}^{(+)}]^{\dagger}$ is the corresponding lowering operator. The off-diagonal terms, $g_{\alpha\beta}(\mathbf{r}_{ij})$, represent the resonant dipole-dipole interaction [17–19] also obtained in classical electrodynamics [20]:

$$g_{\alpha\beta}(\mathbf{r}_{ij}) = \frac{3}{2} e^{ik_0 r_{ij}} \left[\left(\frac{1}{k_0 r_{ij}} + \frac{i}{(k_0 r_{ij})^2} - \frac{1}{(k_0 r_{ij})^3} \right) \delta_{\alpha\beta} - \left(\frac{1}{k_0 r_{ij}} + \frac{3i}{(k_0 r_{ij})^2} - \frac{3}{(k_0 r_{ij})^3} \right) \frac{r_{ij,\alpha} r_{ij,\beta}}{r_{ij}^2} \right], \quad (5)$$

where $r_{ij} = |\mathbf{r}_i - \mathbf{r}_j|$ and $r_{ij,\alpha}$ is the projection of \mathbf{r}_{ij} on the α direction.

Averaging (5) over the random orientations of the pairs of atoms gives

$$g(r_{ij}) = \frac{e^{ik_0 r_{ij}}}{k_0 r_{ij}}, \quad (6)$$

where we used $\langle \frac{r_{ij,\alpha} r_{ij,\beta}}{r_{ij}^2} \rangle = \frac{1}{3} \delta_{\alpha\beta}$.

This result is also obtained in the scalar case, where the atoms are coupled to a scalar radiation field [21, 22].

IV. COLLECTIVE EMISSION RATES

The cooperative spontaneous emission rates of the atoms are determined by the time evolution of the ground state population obtained from the reduced atomic density matrix ρ_A of the gas [7, 8, 23]:

$$\frac{d\rho_{GG}}{dt} = \Gamma_0 \sum_{ij} \sum_{\alpha\beta} \Lambda_{\alpha\beta}(\mathbf{r}_{ij}) \langle G | S_{j,\alpha}^{(-)} \rho_A S_{i,\beta}^{(+)} | G \rangle, \quad (7)$$

where $\rho_{GG} = \langle G | \rho_A | G \rangle$, $|G\rangle = |g_1, \dots, g_i, \dots, g_N\rangle$, and the reduced atomic density matrix is obtained from tracing the density matrix over the radiation degrees of freedom. The random matrix $\Lambda_{\alpha\beta}(\mathbf{r}_{ij})$ is the imaginary part of the resonant dipole-dipole interaction (5), namely, $\Lambda_{\alpha\beta}(\mathbf{r}_{ij}) \equiv \text{Im}[g_{\alpha\beta}(\mathbf{r}_{ij})]$.

We denote the n -th dimensionless eigenvalue of $\Lambda_{\alpha\beta}(\mathbf{r}_{ij})$ by Γ_n and the associated n -th eigenfunction by $u_i^{(n)}$. Using the orthonormality of the eigenfunctions, we can rewrite (7) as

$$\frac{d\rho_{GG}}{dt} = \Gamma_0 \sum_{n=1}^{3N} \Gamma_n \langle G | S_n^{(-)} \rho_A S_n^{(+)} | G \rangle, \quad (8)$$

where the collective raising and lowering operators are $S_n^{(\pm)} = \sum_{i=1}^N \sum_{\alpha} u_i^{(n)} S_{i,\alpha}^{(\pm)}$.

Thus, it is possible to interpret the eigenvalues of the random matrix $\Lambda_{\alpha\beta}(\mathbf{r}_{ij})$ as the cooperative spontaneous emission rates of the atoms (in units of Γ_0), i.e., the photon escape rates from the atomic gas [7, 8].

In the vectorial case, the $3N \times 3N$ coupling matrix is

$$\Lambda_{\alpha\beta}(\mathbf{r}_{ij}) = \frac{3}{2} \left[\left(\frac{\sin(k_0 r_{ij})}{k_0 r_{ij}} + \frac{\cos(k_0 r_{ij})}{(k_0 r_{ij})^2} - \frac{\sin(k_0 r_{ij})}{(k_0 r_{ij})^3} \right) \delta_{\alpha\beta} - \left(\frac{\sin(k_0 r_{ij})}{k_0 r_{ij}} + 3 \frac{\cos(k_0 r_{ij})}{(k_0 r_{ij})^2} - 3 \frac{\sin(k_0 r_{ij})}{(k_0 r_{ij})^3} \right) \frac{r_{ij,\alpha} r_{ij,\beta}}{r_{ij}^2} \right], \quad (9)$$

while in the scalar case the $N \times N$ coupling matrix is given by

$$\Lambda(r_{ij}) = \frac{\sin(k_0 r_{ij})}{k_0 r_{ij}}. \quad (10)$$

The properties of (10) have been studied in detail, both numerically [9] and analytically [9, 24]. In the following sections we study numerically the vectorial coupling matrix (9) and compare the obtained results to those of the scalar case.

The average density of eigenvalues of Λ is

$$P(\Gamma) = \frac{1}{M} \overline{\sum_{n=1}^M \delta(\Gamma - \Gamma_n)}, \quad (11)$$

where $M = 3N$ (resp. N) in the vectorial (resp. scalar) case. The average, denoted by $\overline{\quad}$, is taken over the spatial random configurations of the atoms.

We examine two limiting cases. In the dilute gas limit ($k_0 r_{ij} \gg 1$), $\Lambda_{\alpha\beta}(\mathbf{r}_{ij}) = \delta_{ij}\delta_{\alpha\beta}$ and $\Lambda(r_{ij}) = \delta_{ij}$. Thus,

$$P(\Gamma) = \delta(\Gamma - 1), \quad (12)$$

and the single-atom spontaneous emission rate is recovered in both the vectorial and scalar cases.

In the so-called Dicke limit ($k_0 r_{ij} \ll 1$), $\Lambda_{\alpha\beta}(\mathbf{r}_{ij}) = \delta_{\alpha\beta}$ and $\Lambda(r_{ij}) = 1$. Therefore, for both the vectorial and scalar cases,

$$P(\Gamma) = \frac{1}{N} [\delta(\Gamma - N) + (N - 1)\delta(\Gamma)]. \quad (13)$$

Here, $\Gamma = N$ is the non-degenerate superradiant mode, while $\Gamma = 0$ is the $(N - 1)$ -degenerate subradiant mode.

It should be noted that the mean value of Γ hardly characterizes $P(\Gamma)$ since $\Gamma_{mean} = [\text{Tr}(\Lambda)]/M$ and $\text{Tr}(\Lambda) = M$ in both the vectorial and scalar cases, thus $\Gamma_{mean} = 1$ regardless of the system parameters.

Therefore, in order to characterize $P(\Gamma)$ and obtain a measure of photon localization we use the following function:

$$C = 1 - 2 \int_1^\infty d\Gamma P(\Gamma), \quad (14)$$

normalized to unity. The function C measures the relative number of states having a vanishing escape rate. In the dilute gas limit, (12) implies that $C = 0$, indicating photon delocalization [25]. In the Dicke limit, (13) gives

$$C = 1 - \frac{2}{N}. \quad (15)$$

Thus, for $N \gg 1$, $C = 1$ and photons are localized in the gas.

In the scalar case, away from the Dicke limit, the function C has been thoroughly studied. It exhibits a scaling behavior over a broad range of system size and density in one [14], two [12], and three dimensions [9]. In three dimensions, C can be approximated asymptotically by

$$C \simeq 1 - 3 \frac{N_\perp}{N}, \quad (16)$$

where $N_\perp \equiv (k_0 L)^2/4$ is the number of transverse photon modes in an atomic volume L^3 .

In the next sections we study C in the vectorial case and show that it exhibits a scaling behavior and obeys (16) as well.

V. METHOD

In order to obtain $P(\Gamma)$ and C in the vectorial case beyond the two limits discussed in the previous section, we follow [9]. We consider $N \gg 1$ atoms enclosed in a cubic volume L^3 . The atoms are distributed with a uniform density $\rho = N/L^3$. Using the resonant radiation wavelength, $\lambda = 2\pi/k_0$, we define the dimensionless density $\rho\lambda^3$. Next, we introduce the Ioffe-Regel number [26], $k_0 l$, where l is the photon elastic mean free path, namely $l = 1/\rho\sigma$ and σ is the average single scattering cross section. For resonant scattering, the scattering cross section varies as λ^2 , so that the Ioffe-Regel number can be written as $k_0 l^{(s)} = 2\pi^2/\rho\lambda^3$ in the scalar case and $k_0 l^{(v)} = (2/3)k_0 l^{(s)}$ in the vectorial case [27]. Finally, we define the (on resonance) optical thickness, b_0 , as the ratio between the system size L and the photon elastic mean free path l . Using the definitions above, one obtains $b_0^{(s)} = N^{1/3}(\rho\lambda^3)^{2/3}/\pi$ and $b_0^{(v)} = (3/2)b_0^{(s)}$. It is important to note that the optical thickness is related to the number of transverse photon modes by $b_0^{(s)} = \pi N/N_\perp$ and $b_0^{(v)} = (3\pi/2)N/N_\perp$. Thus, b_0 is the scaling parameter in (16).

While the Ioffe-Regel number accounts for disorder effects, cooperative effects are better described by the optical thickness [6, 9, 28, 29]. Therefore, we will use these two parameters to investigate the distinctive roles of disorder and cooperative effects in atomic gases.

For a given spatial atomic configuration, we numerically calculate the $3N$ eigenvalues of (9) in vectorial case, and, for comparison, the N eigenvalues of (10) in the scalar case. By varying the spatial configuration of the scatterers and averaging over disorder we obtain (11) and (14).

VI. PHOTON ESCAPE RATE DISTRIBUTION

In this section we study $P(\Gamma)$ in the vectorial case and compare the results to the scalar case, both for the large sample regime ($L > \lambda$) and the small sample regime ($L \ll \lambda$).

A. Large sample regime

We first consider the photon escape rate distributions in the large sample size limit ($L > \lambda$). Figure 1 shows the photon escape rate distribution $P(\Gamma)$ for a gas of $N = 700$ atoms with increasing spatial densities. The results

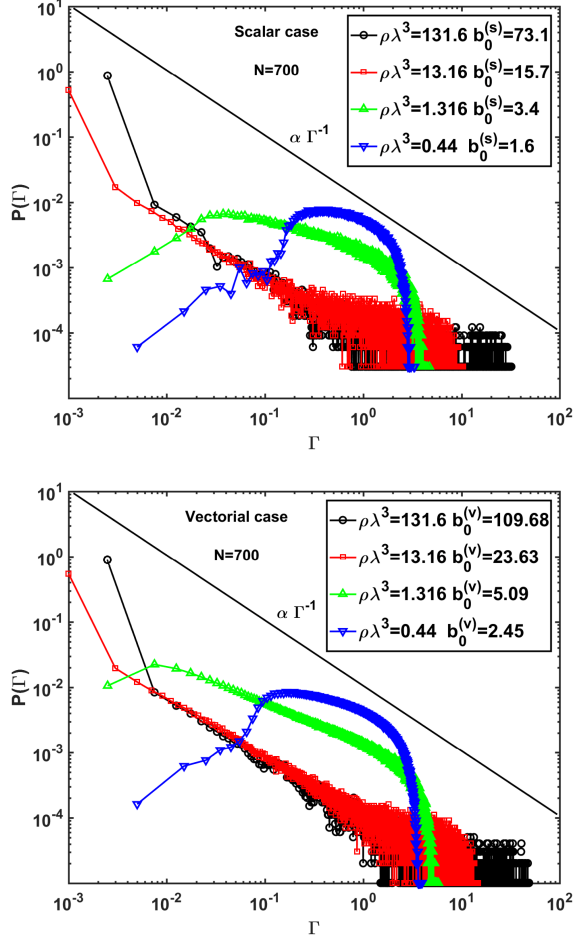


FIG. 1: (Color online) Photon escape rate distribution $P(\Gamma)$ (large sample regime) for $N = 700$ atoms in the scalar (top) and vectorial (bottom) cases for various cloud densities $\rho\lambda^3$.

show that the distribution is qualitatively the same for both the scalar and the vectorial cases. For dilute gases, the distributions are peaked around the single atom decay rate, $\Gamma = 1$, as predicted by (12).

When increasing the density, we observe that $P(\Gamma)$ is shifted toward lower values of Γ , indicating the existence of long-living modes of the photon inside the sample. For dense clouds, when the optical thickness is large enough, the distribution in both cases is well described by the $P(\Gamma) \sim \Gamma^{-1}$ power law, as suggested for the scalar case in [5].

Figure 2 shows the distribution $P(\Gamma)$ at a fixed optical thickness for various spatial densities of scatterers. In both cases, for large enough densities, the photon escape rate obeys the power law of $P(\Gamma) \sim \Gamma^{-1}$.

Next, we consider the configuration-averaged maximal resonance width, Γ_{max} . Figure 3 shows the behavior of Γ_{max} as a function of the optical thickness rescaled by the spatial density of the gas for both the scalar and vectorial cases. No qualitative differences between the scalar and vectorial cases are observed, and in both cases the

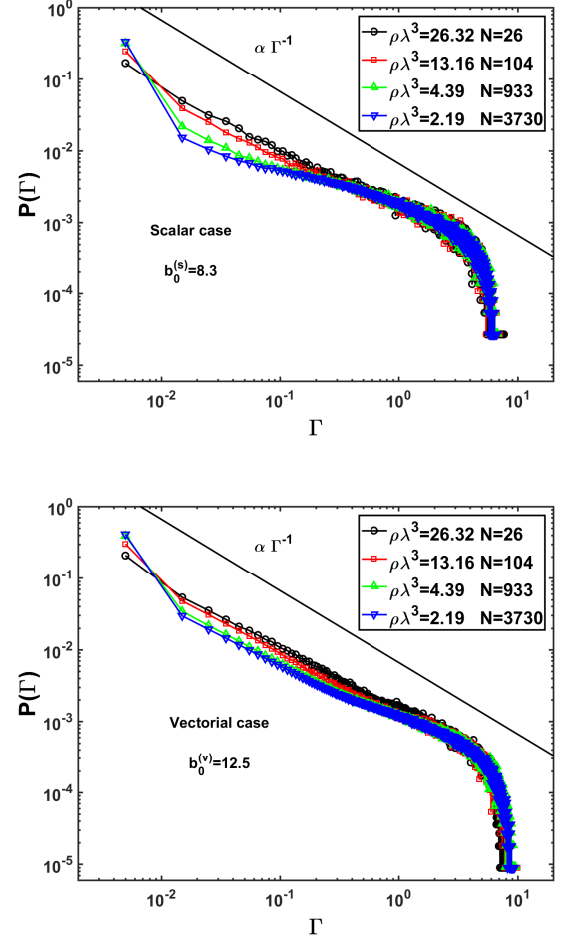


FIG. 2: (Color online) Photon escape rate distribution $P(\Gamma)$ (large sample regime) at a fixed optical thickness ($b_0^{(s)} = 8.30$ and $b_0^{(v)} = 12.50$) in the scalar (top) and vectorial (bottom) cases for various cloud densities $\rho\lambda^3$.

configuration-averaged maximal resonance width follows the expression:

$$\Gamma_{max}^{(s,v)} = \sqrt{\frac{b_0^{(s,v)} - 2/k_0 l^{(s,v)}}{A} + \left(\frac{b_0^{(s,v)} - 2/k_0 l^{(s,v)}}{B}\right)^2 + \frac{b_0^{(s,v)} - 2/k_0 l^{(s,v)}}{C} + 1}, \quad (17)$$

where $A = 1.00$, $B = 5.00$, and $C = 4.50$ are free fitting parameters obtained numerically.

Equation (17) indicates that Γ_{max} is dominated by cooperative effects, depending on the optical thickness, and slightly corrected by disorder effects, depending on the spatial density of the cloud. This equation recovers the asymptotic behavior predicted by the Marchenko-Pastur law [24, 30], namely $\Gamma_{max} \propto \sqrt{b_0 - 2/k_0 l}$ for dilute gases, and $\Gamma_{max} \propto b_0 - 2/k_0 l$ for dense clouds.

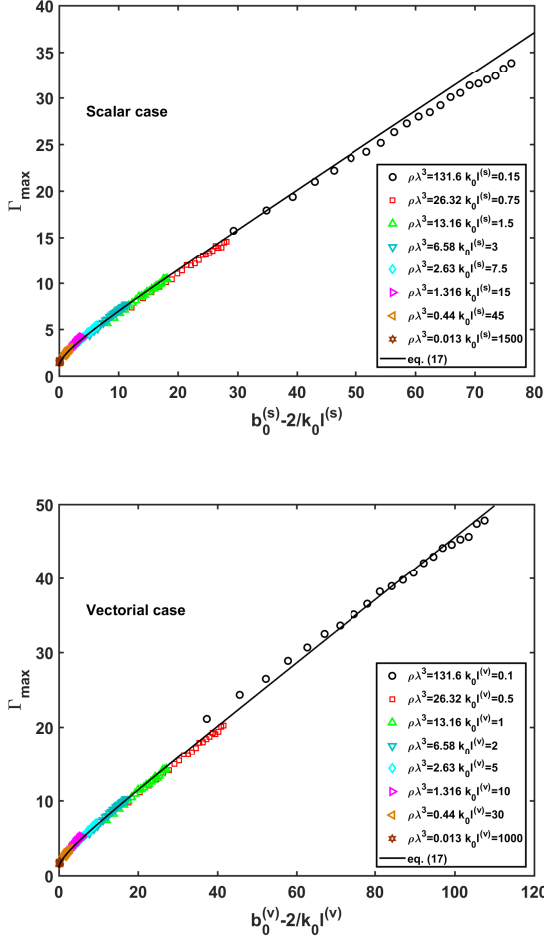


FIG. 3: (Color online) Maximal resonance width Γ_{max} (large sample regime) in the scalar (top) and vectorial (bottom) cases. The solid line is given by (17) in both cases.

B. Small sample regime

Figure 4 shows the photon escape rate distribution in the small sample regime for a cloud of $N = 100$ atoms enclosed in a system of size $k_0 L = 0.266$ in the scalar and vectorial cases. In both cases, we observe the superradiant mode situated at $\Gamma = N$ and the subradiant modes close to $\Gamma = 0$, as predicted by (13).

VII. SCALING FUNCTION

Figure 5 shows the behavior of C defined in (14) as a function of the system size ($L > \lambda$) for increasing atomic densities in the scalar and vectorial cases. No significant differences are observed between the two cases. For dilute (or optically thin) gases, $P(\Gamma)$ is peaked around the single atom decay rate, so that $C \rightarrow 0$. For dense (or optically thick) media, according to Section VI, $P(\Gamma)$ is shifted

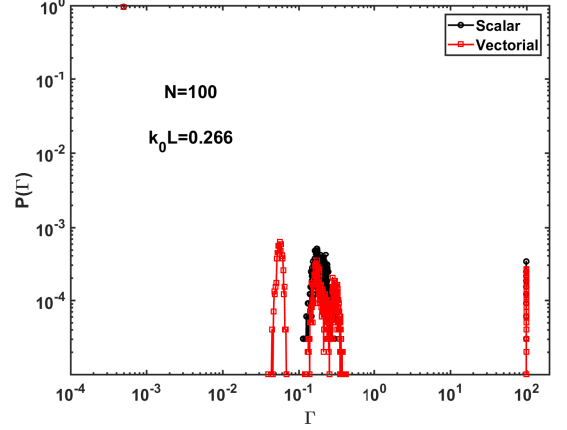


FIG. 4: (Color online) Photon escape rate distribution $P(\Gamma)$ in the scalar (black circles) and vectorial (red squares) cases for $N = 100$ atoms enclosed in a system of size $k_0 L = 0.266$.

toward lower values of Γ , hence $C \rightarrow 1$.

The data of Fig. 5 (both in the scalar and vectorial cases) collapse on a single curve (Fig. 6) when plotted as a function of the optical thickness, indicating that photons undergo a crossover from delocalization toward localization as the scaling variable b_0 is increased. Therefore, photon localization is dominated by cooperative effects rather than disorder. In both cases, the numerical data are in line with the theoretical expression (16).

The obtained result that the scaling function increases with the optical thickness can be explained as follows. As the number of scattering events is increased, it takes more time for the photon to leave the gas, thus the relative number of states having a vanishing escape rate is increased.

In the small sample regime ($L \ll \lambda$), the behavior of the function C is shown in Fig. 7 for the scalar and vectorial cases. In both cases, the numerical data are in full agreement with the theoretical prediction (15).

VIII. DISCUSSION

We have studied the photon escape rate distribution from an ensemble of random atomic scatterers coupled to a scalar or vector radiation field. It has been shown that in both cases the results are qualitatively the same. Moreover, in these two cases, the function C exhibits a scaling behavior over a broad range of system parameters, where the optical thickness serves as the scaling parameter (in the large sample regime). This observation is in line with the findings reported by the authors of [9], who originally calculated the scaling function in the scalar case. The finding that photons undergo a crossover from delocalization toward localization rather than a disorder-driven phase transition as expected from

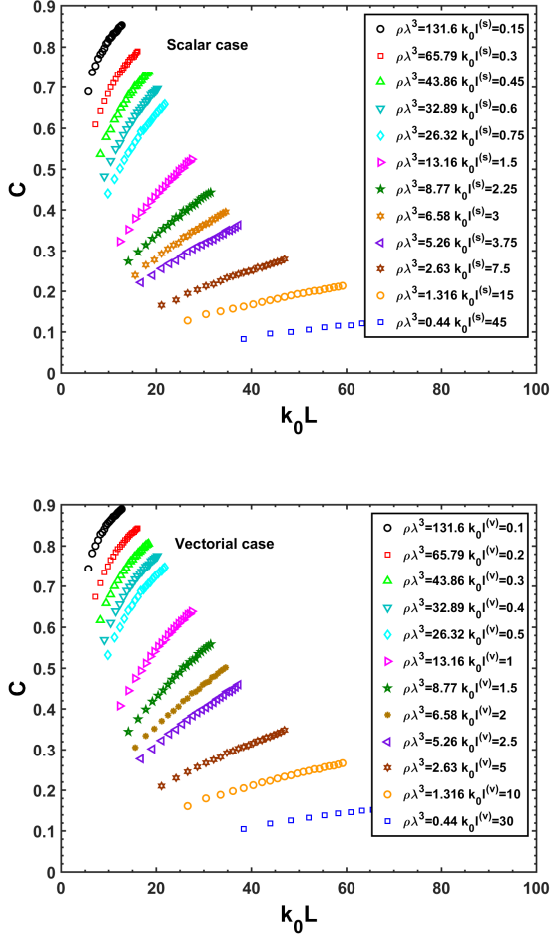


FIG. 5: (Color online) C as a function of the system size $k_0 L$ (large sample regime) for increasing atomic densities $\rho \lambda^3$ in the scalar (top) and vectorial (bottom) cases.

Anderson localization [13], suggests that photon localization is dominated by cooperative effects rather than disorder.

The results show that the scalar model, which ignores the vectorial nature of light, is an excellent approximation when considering photon escape rates from atomic gases. As the scalar model is much simpler compared to the vectorial one, the former could be used, without losing substantial information. Since averaging the vectorial coupling matrix $\Lambda_{\alpha\beta}(\mathbf{r}_{ij})$ (9) over the random orientations of the atoms leads to the scalar coupling matrix $\Lambda(r_{ij})$ (10), our results indicate that $P(\Gamma)$ is not sensitive to the detailed location of the atoms.

It is interesting to compare our findings to those obtained when diagonalizing the effective Hamiltonian, namely calculating the spectrum of $g_{\alpha\beta}(\mathbf{r}_{ij})$ (5) in the vectorial case and $g(r_{ij})$ (6) in the scalar case. When taking into account the real part of g as well, there are significant differences between the scalar and vectorial cases, as pointed out by [2]. The real part of g is re-

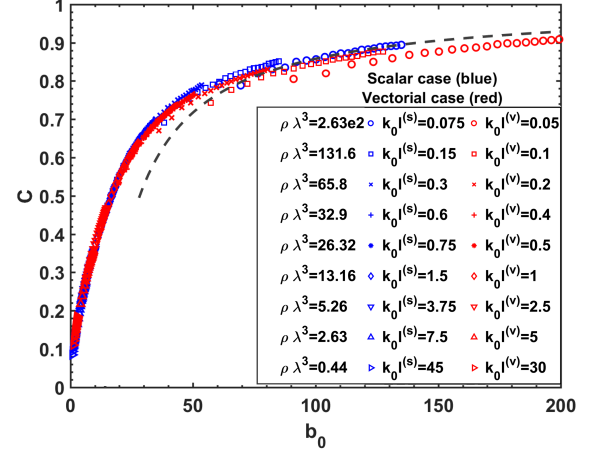


FIG. 6: (Color online) C as a function of the optical thickness b_0 (large sample regime) for increasing atomic densities $\rho \lambda^3$ in the scalar (blue) and vectorial (red) cases. In both cases, the dashed line is given by (16).

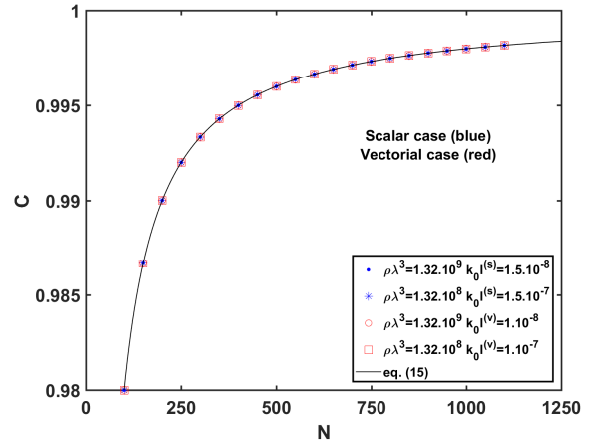


FIG. 7: (Color online) C as a function of the number of atoms N (small sample regime) for the scalar (blue) and vectorial (red) cases. The solid lines is given by (15) in both cases. For a density of $\rho \lambda^3 = 1.32 \cdot 10^8$, the system size is $0.06 \leq k_0 L \leq 0.13$, and for a density of $\rho \lambda^3 = 1.32 \cdot 10^9$, the system size is $0.03 \leq k_0 L \leq 0.06$.

sponsible for van der Waals dephasing, a phenomenon that is sensitive to the detailed location of the scatterers [31]. Therefore, when dealing with the spectrum of the effective Hamiltonian, the orientation-averaged scalar model is essentially different from the vector model. In the study described in this paper, only the imaginary part of g is relevant and van der Waals dephasing does not play a role. Hence, the detailed location of the atoms is less important and an orientation-averaged calculation constitutes a very good approximation.

IX. CONCLUSIONS

We have numerically studied photon escape rates from three-dimensional atomic gases, while taking into account the vectorial nature of light. We have shown that the vector and scalar models qualitatively follow the same scaling law. In both cases, photons undergo a

crossover from delocalization toward localization as the optical thickness of the cloud is increased. Therefore, photon localization is dominated by cooperative effects rather than disorder. This theoretical conclusion calls for the identification of experimental signatures allowing to distinguish between the two mechanisms of photon localization.

-
- [1] S. E. Skipetrov and I. M. Sokolov, Phys. Rev. Lett. **112**, 023905 (2014).
 - [2] L. Bellando, A. Gero, E. Akkermans, and R. Kaiser, Phys. Rev. A **90**, 063822 (2014).
 - [3] S. E. Skipetrov and I. M. Sokolov, Phys. Rev. Lett. **114**, 053902 (2015).
 - [4] S. E. Skipetrov, Phys. Rev. Lett. **121**, 093601 (2018).
 - [5] F. A. Pinheiro, M. Rusek, A. Orlowski, and B. A. van Tiggelen, Phys. Rev. E **69**, 026605 (2004).
 - [6] T. Bienaimé, N. Piovella, and R. Kaiser, Phys. Rev. Lett. **108**, 123602 (2012).
 - [7] E. Ressayre and A. Tallet, Phys. Rev. Lett. **37**, 424 (1976).
 - [8] E. Ressayre and A. Tallet, Phys. Rev. A **15**, 2410 (1977).
 - [9] E. Akkermans, A. Gero, and R. Kaiser, Phys. Rev. Lett. **101**, 103602 (2008).
 - [10] P. W. Anderson, Phys. Rev. **109**, 1492 (1958).
 - [11] R. H. Dicke, Phys. Rev. **93**, 99 (1954).
 - [12] A. Gero and E. Akkermans, Phys. Rev. A **88**, 023839 (2013).
 - [13] E. Abrahams, P. W. Anderson, D. C. Licciardello, and T. V. Ramakrishnan, Phys. Rev. Lett. **42**, 673 (1979).
 - [14] E. Akkermans and A. Gero, Europhys. Lett. **101**, 54003 (2013).
 - [15] K. Ellinger, J. Cooper, and P. Zoller, Phys. Rev. A **49**, 3909 (1994).
 - [16] O. Morice, Y. Castin, and J. Dalibard, Phys. Rev. A **51**, 3896 (1995).
 - [17] M. J. Stephen, J. Chem. Phys. **40**, 669 (1964).
 - [18] R. H. Lehman, Phys. Rev. A **2**, 883 (1970).
 - [19] P. W. Milonni and P. L. Knight, Phys. Rev. A **10**, 1096 (1974).
 - [20] J. Jackson, *Classical Electrodynamics* (Wiley, 1998).
 - [21] A. Gero and E. Akkermans, Phys. Rev. Lett. **96**, 093601 (2006).
 - [22] A. Gero and E. Akkermans, Phys. Rev. A **75**, 053413 (2007).
 - [23] V. Ernst and P. Stehle, Phys. Rev. **176**, 1456 (1968).
 - [24] S. E. Skipetrov and A. Goetschy, J. Phys. A: Math. Theor. **44**, 065102 (2011).
 - [25] The δ function is considered as a limiting case of an even function peaked at zero. Thus, the integral of $\delta(x)$ from 0 to infinity equals 1/2.
 - [26] A. F. Ioffe and A. R. Regel, Prog. Semicond. **4**, 237 (1960). For historical reasons mainly, the dimensionless quantity $k_0 l$ is often called the Ioffe-Regel number.
 - [27] E. Akkermans and G. Montambaux, *Mesoscopic Physics of Electrons and Photons* (Cambridge University Press, England, 2007), Section 6.6.
 - [28] G.-D. Lin and S. F. Yelin, Phys. Rev. A **85**, 033831 (2012).
 - [29] G.-D. Lin and S. F. Yelin, Molec. Phys. **111**, 1917 (2013).
 - [30] V. A. Marchenko and L. A. Pastur, Mat. Sbornik USSR **1**, 457 (1967).
 - [31] M. Gross and S. Haroche, Phys. Rep. **93**, 301 (1982).